AJNR

The Jugular Foramen: Imaging Strategy and Detailed Anatomy at 3T

J. Linn, F. Peters, B. Moriggl, T.P. Naidich, H. Brückmann and I. Yousry

AJNR Am J Neuroradiol published online 2 October 2008
http://www.ajnr.org/content/early/2008/10/02/ajnr.A1281.citation

Published October 2, 2008 as 10.3174/ajnr.A1281

ORIGINAL RESEARCH

The Jugular Foramen: Imaging Strategy and Detailed Anatomy at 3T

J. Linn
F. Peters
B. Moriggl
T.P. Naidich
H. Brückmann
I. Yousry

BACKGROUND AND PURPOSE: The purpose of this study was to assess how well the anatomy of the jugular foramen (JF) could be displayed by 3T MR imaging by using a 3D contrast-enhanced fast imaging employing steady-state acquisition sequence (CE-FIESTA) and a 3D contrast-enhanced MR angiographic sequence (CE-MRA).

MATERIALS AND METHODS: Twenty-five patients free of skull base lesions were imaged on a 3T MR imaging scanner using CE-FIESTA and CE-MRA. Two readers analyzed the images in collaboration, with the following objectives: 1) to score the success with which these sequences depicted the glossopharyngeal (CNIX) and vagus (CNX) nerves, their ganglia, and the spinal root of the accessory nerve (spCNXI) within the JF, and 2) to determine the value of anatomic landmarks for the in vivo identification of these structures.

RESULTS: CE-FIESTA and CE-MRA displayed CNIX in 90% and 100% of cases, respectively, CNX in 94% and 100%, and spCNXI in 51% and 0% of cases. The superior ganglion of CNIX was discernible in 89.8% and 87.8%; the inferior ganglion of CNIX, in 73% and 100%; and the superior ganglion of CNX, in 98% and 100% of cases. Landmarks useful for identifying these structures were the inferior petrosal sinus and the external opening of the cochlear aqueduct.

CONCLUSIONS: This study protocol is excellent for displaying the complex anatomy of the JF and related structures. It is expected to aid in detecting small pathologies affecting the JF and in planning the best surgical approach to lesions affecting the JF.

The jugular foramen (JF) is a bony channel that transmits vessels and cranial nerves IX, X, and XI (CNIX, CNX, and CNXI) through the skull base into the carotid space.[1] It can be divided into 3 compartments[1]: 1) a neural compartment, containing the CNIX to CNXI; 2) a larger venous compartment (sigmoid part), containing the sigmoid sinus; and 3) a smaller venous compartment (petrosal part), containing the inferior petrosal sinus. The sigmoid and the petrosal parts are separated by bony processes: the intrajugular processes, which originate from the opposing surfaces of the temporal and occipital bones, as well as by a dural septum, which connects these 2 bony structures.[1]

The lower cranial nerves enter the JF via 2 dural meatuses: the glossopharyngeal meatus for the glossopharyngeal nerve (CNIX) and the vagal meatus for both the vagus nerve (CNX) and the accessory nerve (CNXI). CNIX and CNX each possess both a superior (supCNIX and supCNX) and an inferior ganglion (infCNIX and infCNX). While the supCNIX, the infCNIX, and the supCNX lie within the JF, the infCNIX is located more caudally.[2,3] The cranial nerve roots of CNXI (crCNXI) intermingle with the roots of CNX within the JF, so their fibers are classified together as the CNX/XI complex.[1] The spinal root of CNXI (spCNXI) traverses the JF in the same dural sheath as CNX, but remains separate from it.[4] Just inferior to its dural meatus, CNIX turns forward and then sharply downward forming the so-called "genu" of CNIX.[1]

Despite extensive cadaveric dissection studies, which have addressed the anatomy of the JF, many details on the in vivo anatomy of the JF remain unclear.[1-7] Due to its complexity, to our knowledge, the JF anatomy has not yet been systematically evaluated in imaging studies, though this knowledge would be highly important for presurgical planning.

To date, high-resolution MR imaging provides a noninvasive tool, which should enable us to depict the exact location of the intraforaminal structures in vivo. Recent studies showed that contrast-enhanced steady-state and MR angiography (MRA) sequences are suitable techniques to image the intraforaminal segments of other cranial nerves,[7,8] but not yet CNIX–CNXI. Therefore, we hypothesized that a contrast-enhanced 3D fast imaging employing steady-state acquisition sequence (CE-FIESTA) and a high-resolution contrast-enhanced gradient-echo MRA (CE-MRA) technique, performed on a 3T MR imaging scanner, should be valuable for the identification of the JF and its contents.

Thus, we aimed to determine the potential of these sequences in providing detailed information on the MR imaging anatomy of the JF.

Materials and Methods

Patients

The study group comprised 25 patients (16 women; mean age, 50 ± 17 years) in whom contrast-enhanced MR imaging was performed for unrelated reasons and who agreed to undergo additional CE-FIESTA and CE-MRA sequences. None of these patients had known clinical abnormalities affecting the skull base or the infratentorial region. Furthermore, we present 1 illustrative case of a patient with a meningi-

Received June 10, 2008; accepted July 12.

From the Department of Neuroradiology (J.L., F.P., H.B., I.Y.), University Hospital Munich, Munich, Germany; Institute of Anatomy, Histology, and Embryology (B.M.), Medical University Innsbruck, Austria; and Department of Radiology, Section of Neuroradiology (T.P.N.), Mount Sinai Medical Center, New York, NY.

Paper previously presented in part at: European Congress of Radiology, March 8, 2008; Vienna, Austria; Deutschen Röntgenkongress, October 17–19, 2008; Berlin, Germany; and Jahrestagung der Deutschen Gesellschaft für Neurochirurgie, September 20, 2008; Würzburg, Germany.

Please address correspondence to Jennifer Linn, MD, Department of Neuroradiology, University Hospital Munich, Marchioninistr 15, D-81377 Munich, Germany; e-mail: linn@nrad.de

DOI 10.3174/ajnr.A1281

Table 1: Sequence parameters

	CE-FIESTA	CE-MRA
TR (s)	4.5	6.6
TE (s)	1.8	2.3
FOV (mm)	160	180
Flip angle (°)	50	20
Matrix (mm)	256 × 256	450 × 450
Section thickness (mm)	0.6	0.8
NEX	2	1.15
Resolution (mm)	0.6 × 0.6 × 0.6	0.4 × 0.4 × 0.8
Duration (min:s)	7:45	7:15

Note:—CE-FIESTA indicates contrast-enhanced fast imaging employing steady-state acquisition; CE-MRA, contrast-enhanced MR angiography.

oma affecting the lower cranial nerves and the JF to illustrate the clinical relevance of these MR images.

The study was approved by the review board of our department and conformed to the Helsinki declaration. All patients gave informed consent to participate before beginning the study.

MR Imaging

Imaging was performed on a 3T MR imaging scanner by using an 8-channel high-definition head coil (GE Healthcare, Milwaukee, Wis). The imaging protocol consisted of a CE-MRA and a CE-FIESTA sequence. The CE-MRA was performed first and started 30 seconds after the administration of 0.1-mmol/kg gadobenate dimeglumine (sequence parameters are given in Table 1).

Image Analysis

The 3D datasets from both sequences were analyzed collaboratively by 2 experienced neuroradiologists on a standard workstation by using the multiplanar reconstruction function. Ratings were reached by consensus. The left and right sides of each patient were assessed separately.

The certainty of identifying each anatomic structure was scored on both MR images separately and recorded on an arbitrary scale of 0–2 (identified with certainty, 2; most probably identified, 1; and not identified, 0[9]).

Intraforaminal Compartments. To assess the value of the 2 sequences in depicting the different intraforaminal compartments, we identified the intrajugular processes of the temporal and occipital bones and the dural septum between them. The maximum anteroposterior and transverse dimensions of the sigmoid compartment and the maximum diameter of the inferior petrosal sinus proximal to its drainage into the petrosal portion of the JF were measured on transverse reconstructed planes of the CE-MRA.

CNIX, CNX/XI, and spCNXI within the JF. The exact position of the nerves within the neural compartment, their spatial relationships to each other, and the visualization of a "genu" of CNIX were also assessed.

Ganglia of CNIX and supCNX. The success of identifying the cranial nerve ganglia was scored as follows: A score of 2 was assigned if the ganglion was discernible as a circumscribed thickening of the appropriate cranial nerve. A score of 1 was assigned if no thickening of the nerve was depicted but the nerve itself could be identified with certainty at the anatomic site of its ganglion. A score of 0 was assigned if neither the ganglion nor the nerve could be identified at the appropriate site.

For the identification of the supCNIX, we used 2 landmarks: 1) the external opening of the cochlear aqueduct[1,10] and 2) the "genu" of CNIX.[1]

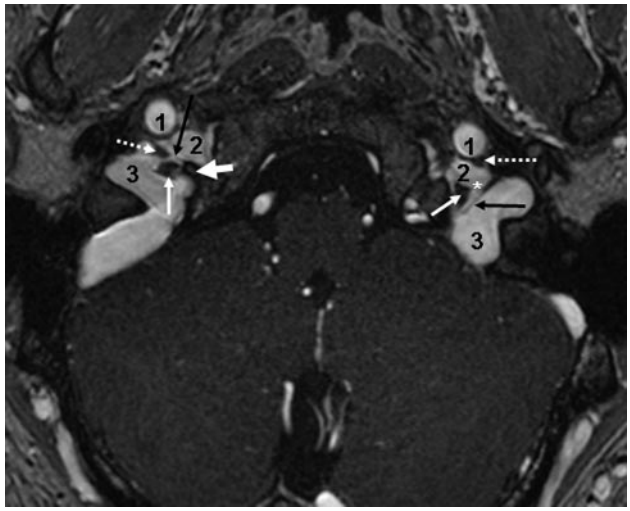

Fig 1. Petrosal and sigmoid parts of the JF. Axial CE-MRA image demonstrates the petrosal and sigmoid parts of the JF as well as the cranial nerves within the intrajugular compartment. The *thick white arrow* marks the right interjugular process of the occipital bone; the *black arrow* depicts the dural septum between the petrosal and sigmoid part of the JF. *Asterisks* mark the drainage of the inferior petrosal sinus into the jugular bulb between CNIX anterolaterally (*dotted arrows*) and the CNX/XI complex at the level of the supCNX posteromedially (*thin white arrow*). 1 indicates the ICA; 2, the inferior petrosal sinus; 3, the sigmoid sinus.

The infCNIX was identified by its anatomic location approximately 3 mm inferior to the supCNIX.[3] The supCNX was identified by its position immediately caudal and dorsal to the supCNIX.[2,3] The infCNX was not assessed in this study because it lies further caudally along the course of CNX and not within the JF.[1,3]

Cochlear Aqueduct. The maximal width of the external opening of the cochlear aqueduct was measured on an oblique plane that was reconstructed parallel to the course of the aqueduct. The length of the cochlear aqueduct was measured from the external opening of the aqueduct as far proximal as the aqueduct could be traced toward the cochlea (length of the aqueduct).

Adjacent Cranial Nerves: CNVII and CNXII. The certainty of identifying the facial nerve (CNVII) in its course through the temporal bone to the parotid gland and of the canalicular segment of the hypoglossal nerve (CNXII) was assessed. Furthermore, we evaluated whether a single or a duplicated hypoglossal canal was present.

Statistical Analysis

To compare the value of the 2 sequences for the identification of each anatomic structure, we performed the Fisher exact probability test. *P* values $< .05$ were judged to be significant.

Results

Forty-nine of 50 sides were suitable for analysis. In 1 patient, CE-FIESTA revealed an asymptomatic small arachnoid cyst in the perimedullary cistern on the right side, which distorted the cisternal segments of the lower cranial nerves. This single side was excluded from further analysis.

Intraforaminal Compartments

On both sequences, the 3 intraforaminal compartments could be identified by reliably depicting the temporal and occipital intrajugular processes as well as the dural septum separating the petrosal from the sigmoid portion. CE-MRA was superior to CE-FIESTA for identifying the dural septum (89.9% versus

Table 2: Identification of anatomic structures within and adjacent to the jugular foramen*

Anatomic Structure (49 sides)	CE-FIESTA				CE-MRA			
	2	1	0	Total†	2	1	0	Total†
Dural septum	0 (0)	21 (43)	28 (0)	21 (43)	29 (59.1)	15 (30.6)	5 (10.2)	44 (89.9)
Cranial nerves								
CNIX	36 (73.5)	8 (16.3)	5 (10.2)	44 (90)	49 (100)	0 (0)	0 (0)	49 (100)
CNX/XI complex‡	39 (79.6)	7 (14.3)	3 (6.1)	46 (94)	49 (100)	0 (0)	0 (0)	49 (100)
spCNXI	10 (40)	6 (24)	9 (36)	25 (51)	0 (0)	0 (0)	49 (100)	0 (0)
Cochlear aqueduct	49 (100)	0 (0)	0 (0)	49 (100)	33 (67)	16 (33)	0 (0)	49 (100)
Ganglia								
supCNIX	12 (24.5)	32 (65.3)	5 (10.2)	44 (89.9)	13 (26.6)	30 (61.2)	6 (12.2)	43 (87.8)
infCNIX	0 (0)	36 (73)	13 (26.5)	36 (73)	24 (0)	25 (100)	0 (0)	49 (100)
supCNX	0 (0)	48 (98)	2 (4)	48 (98)	0 (0)	49 (100)	0 (0)	49 (100)
Adjacent cranial nerve								
CNVII	33 (67.3)	10 (20.4)	6 (12.2)	43 (87.6)	20 (40.8)	8 (16.3)	21 (42.9)	28 (57.1)
Hypoglossal canal	49 (100)	0 (0)	0 (0)	49 (100)	49 (100)	0 (0)	0 (0)	49 (100)
CNXII within canal	46 (93.9)	3 (6.1)	0 (0)	49 (100)	49 (100)	0 (0)	0 (0)	49 (100)

Note:—sup indicates superior; inf, inferior.
* Data are numbers of sides (percentage).
† Total number of sides (percentage) on which the respective anatomic structure was identified (score of 1 or 2).
‡ The cranial nerve rootlets of CNXI intermingle with CNX inside the JF, and thus these nerves are referred to as the CNX/XI complex.

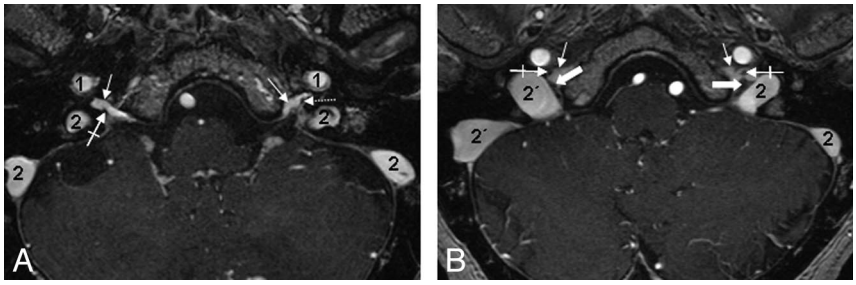

Fig 2. The cranial nerves and their ganglia within the JF. Consecutive axial CE-MRA images from the cranial-to-caudal direction depict the CNIX and the CNX/XI complex within the JF. *A*, The most cranial section is located on the level of the right supCNIX and the left infCNIX (*crossed arrow*). Note that in this case, no circumscript thickening of the nerve is identifiable. Thin *white arrows* indicate the inferior petrosal sinus; 1, the ICA; 2, the sigmoid sinus. *B*, Section at the level of the supCNIX (*thick arrows*). Crossed arrows indicate CNIX within the JF; thin *white arrows*, the inferior petrosal sinus; 1, the ICA; 2, the sigmoid sinus. Note that the right sigmoid part (2′) is significantly larger than the left one (2) in this case.

Table 3: Diameters of the inferior petrosal sinus and sigmoid portion*

Structure	Right Side (mm)	Left Side (mm)
Inferior petrosal sinus†	3.5 (2.3–5.5)	3.6 (2–5.7)
Sigmoid part†		
Anteroposterior	8.7 (8–9.4)	7.7 (6.9–8.5)
Left-right direction	10 (9.3–10.7)	8.8 (8–9.6)

* Data are mean (range).
† Measured on CE-MRA.

43%; Fig 1 and Table 2). The sigmoid portion was significantly larger on the right than on the left side in 60% of patients, whereas there was no significant difference between the mean width of the inferior petrosal sinus on either side (Fig 2 and Table 3).

Cranial Nerves within the Neural Compartment

Both pulse sequences enabled us to identify and differentiate CNIX from CNX/XI within the neural compartment of the jugular fossa (FIESTA, 90% and 94%; CE-MRA, 100% and 100%, respectively). However, the CE-MRA sequence proved to be significantly superior to the CE-FIESTA ($P < .01$; Fig 2 and Table 2). In all cases in which CNIX was discernible within the JF, its genu could also be identified on both sequences.

CE-FIESTA images provided better depiction of the spCNXI than did CE-MRA. On CE-FIESTA images, the spCNXI could be followed from the brain stem through the vagal meatus into the jugular fossa in 51% of sides (Fig 3 and Table 2). On CE-MRA sequences, the spCNXI could not be identified in its cisternal course, so it could not be traced distally. Of the 3 cranial nerves, CNIX was located most anterorolaterally. CNX/XI adjoined it posteromedially. Where identified, the spCNXI lay further posteromedially. The CNX/XI complex typically had a triangular shape on transverse sections (Figs 1 and 2).

Nerve Ganglia

The nerve ganglia could be reliably identified in high percentages on both the CE-FIESTA and CE-MRA sequences: supCNIX, 89.9% and 87.8%; infCNIX, 73% and 100%; supCNX, 98% and 100%, respectively (Figs 1, 2, 4, and 5). CE-MRA was superior to the CE-FIESTA for identifying the infCNIX ($P < .05$). There was no significant difference between the sequences with respect to displaying supCNXI and supCNX (Table 2).

Cochlear Aqueduct

Both sequences depicted the cochlear aqueduct and its external opening on both sides (Table 2). For the dimensions of the cochlear aqueduct, see Table 4.

Cranial Nerves Adjacent to the JF: CNXII and CNVII

The canalicular segments of CNXII could be reliably identified in both sequences (Fig 5 and Table 2). In 5 sides (10.2%), the hypoglossal canal was duplicated (Fig 6); in the remaining

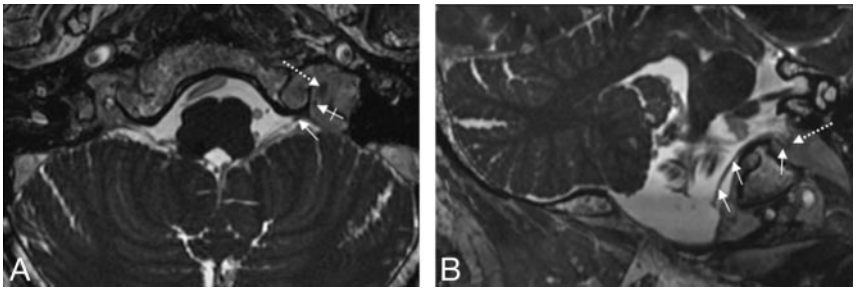

Fig 3. *A* and *B*, Depiction of the spCNXI on FIESTA MR imaging. The spCNXI (*thin white arrows*) is visualized on axial (*A*) and oblique coronal (*B*) FIESTA MR images in its cisternal course (*thin arrows*) and after its entrance into the JF (*crossed arrow*). The *dotted arrow* indicates the CNX/XI complex.

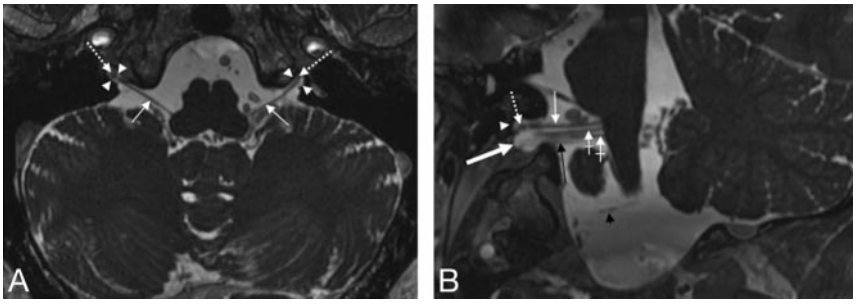

Fig 4. Visualization of the supCNIX. Axial (*A*) and oblique sagittal (*B*) 3D-FIESTA MR images. *B*, The oblique sagittal image is reconstructed parallel to the cisternal course of the lower CNIXs. Nerve root bundles of CNIX (*thin white arrows*), CNX (*crossed white arrows*), crCNXI (*black arrow*), and CNXII (*black arrowhead*) and the glossopharyngeal meatus (*white arrowhead*), vagal meatus (*thick white arrow*), and the supCNXI (*dotted white arrows*) are depicted.

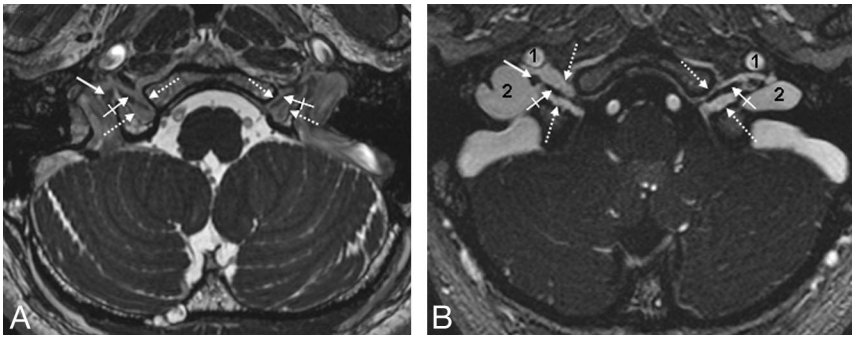

Fig 5. *A* and *B*, CNXII within the hypoglossal canal. Axial FIESTA MR image (*A*) and CE-MRA image (*B*) clearly demonstrate the canalicular segment of CNXII. *Dotted arrows* indicate borders of the hypoglossal canal; *crossed arrow*s, the canalicular segment of CNXII; *thin white arrows*, the CNX/XI complex within the JF; 1, the ICA; 2, the jugular bulb.

Table 4: Dimensions of the cochlear aqueduct*

	Right Side (mm)	Left Side (mm)
Length	6.3 (3.6–9.5)	6.4 (3.8–8.7)
Width of external opening	2.9 (1.2–5.2)	2.8 (2–5.1)

* Data are mean (range) measured on CE-FIESTA.

sides, a single canal was present. CNVII was depicted in its course through the temporal bone to the parotid gland, with the CE-FIESTA being superior to the CE-MRA ($P < .01$, 88% versus 57%; Fig 7 and Table 2).

Illustrative Case

We present a 52-year-old male patient with a left-sided meningioma of the petrosellar ligament, which extends throughout the lateral cerebellomedullary cistern as far caudal as the level of the hypoglossal canal. CE-MRA and FIESTA images depicted the lower cranial nerves and their ganglia with respect to the tumor extension in detail (Fig 8).

Discussion

This is the first 3T MR imaging study to provide detailed information on the anatomy of the JF and its contents. Our results show that combined use of CE-FIESTA and CE-MRA successfully depicts the complex anatomy of the JF, its contents, and adjacent structures.

Although CE-MRA proved to be significantly superior to CE-FIESTA for identifying and differentiating the intraforaminal portions of CNIX and CNX/XI, only the CE-FIESTA sequence differentiated the spCNXI from CNX/XI. Our protocol enabled us to visualize the ganglia of CNIX and CNX within the JF for the first time. Both contrast-enhanced pulse sequences reliably depicted the glossopharyngeal and vagal ganglia, but the CE-MRA was superior to the CE-FIESTA for displaying the infCNIX.

The JF is one of the most complicated anatomic structures of the skull base. Although several anatomic dissection studies have evaluated its anatomy,[1-3] few in vivo imaging studies have been reported in the literature.[9-14] These imaging studies

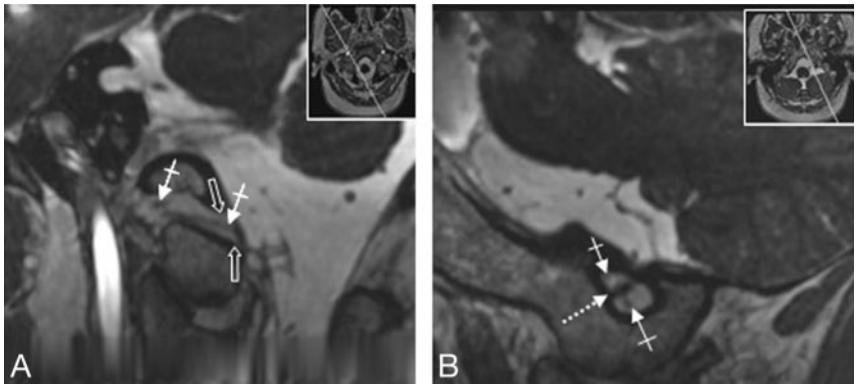

Fig 6. Demonstration of a bilaterally duplicated hypoglossal canal. Oblique reconstructed FIESTA images of a patient with a duplicated hypoglossal canal on both sides. Thumbnails indicate the reconstruction planes. *Open thick arrows* indicate borders of the caudal part of the duplicated canal; *crossed arrows*, the canalicular segments of the hypoglossal nerves. Note that 2 distinct canalicular nerve root bundles can be identified, both of which are demonstrated simultaneously in the images (*crossed arrows*). *B, Dotted arrow* indicates the bony septum between both the cranial and the caudal parts of the duplicated hypoglossal canal.

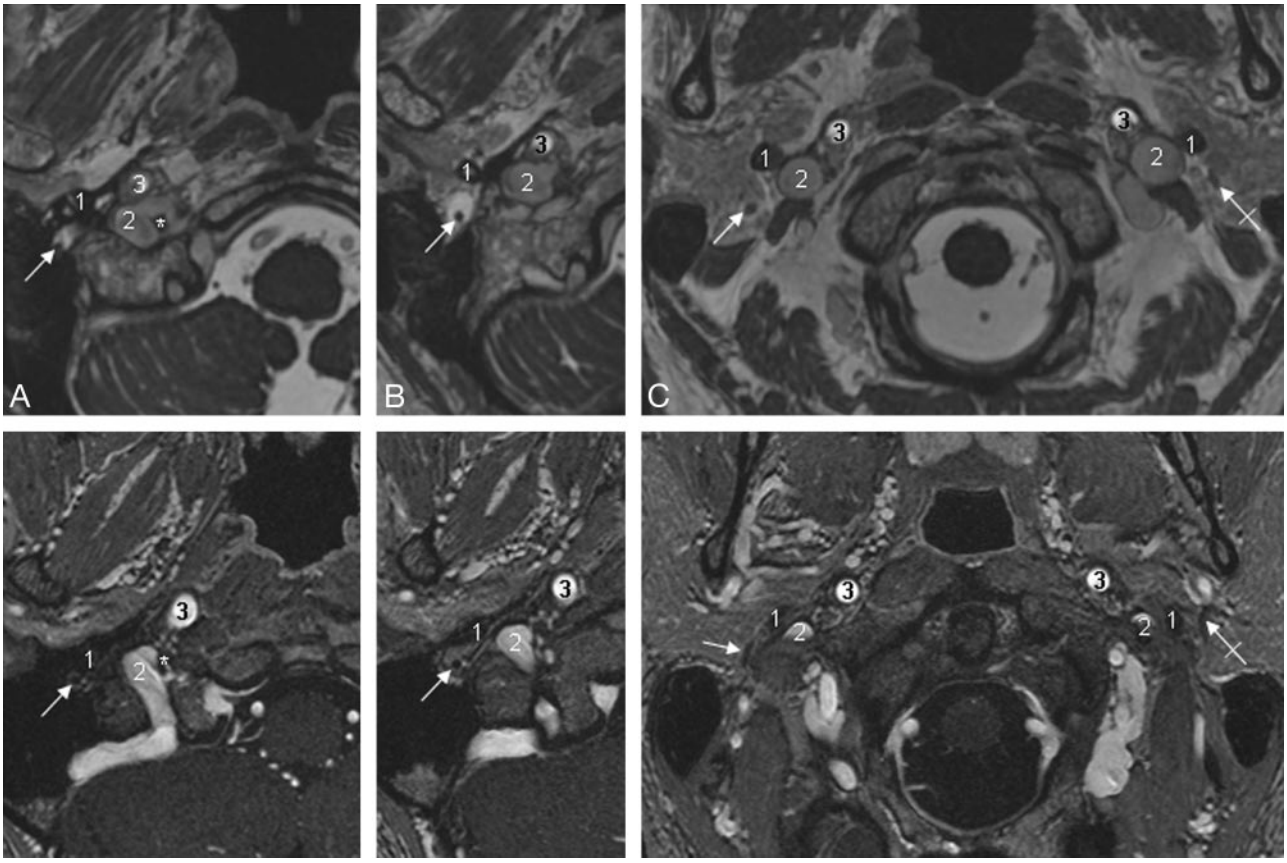

Fig 7. Depiction of CNVII. Axial FIESTA (upper row) and CE-MRA images demonstrate CNVII (*thin white arrows* indicate the right CNVII; *crossed arrows*, the left CNVII) within the stylomastoid foramen (*A*) and in its extracranial course after leaving the temporal bone via the stylomastoid foramen (*B* and *C*). 1 indicates the styloid process of the temporal bone; 2, the sigmoid sinus (*A*) and jugular vein (*B* and *C*), respectively; 3, the ICA.

did not analyze the complex intraforaminal anatomy in detail. Therefore, the diagnosis of intraforaminal pathologic processes remains a challenge. The aim of the present study was to address this problem.

Sequences

Recent studies showed that contrast-enhanced steady-state sequences such as 3D constructive interference in steady-state and 3D FIESTA can be used successfully to image the intraforaminal and cavernous segments of the cranial nerves.[8,15-17] These sequences have usually been used to image the cisternal segments of the cranial nerves.[18-20] When used after intravenous contrast enhancement, however, they also provide sufficient contrast to enhance the venous plexus surrounding the intraforaminal portions of the nerves.[8,15] As a result, the nerves appear as nonenhancing linear structures within the enhancing plexus. By use of these sequences, both the cisternal and the intraforaminal portions of the nerves can be imaged in 1 session.

The image contrast provided by the steady-state sequences

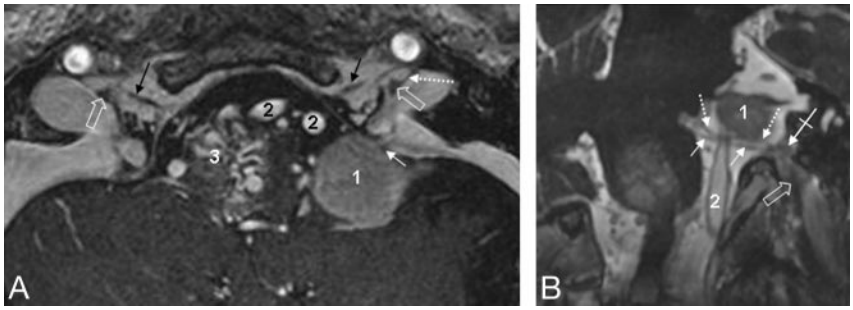

Fig 8. Illustrative clinical case. A 52-year-old male patient with a left-sided meningioma of the petrosellar ligament (marked as 1). *A* and *B*, The meningioma extends throughout the lateral cerebellomedullary cistern as far caudal as the level of the hypoglossal canal. CE-MRA (*A*) and FIESTA (*B*) images allow the detailed depiction of the lower cranial nerves and their ganglia with respect to the tumor extension. *A*, Axial CE-MRA image shows the meningioma (1) which spreads around the spCNXI (*thin white arrow*). Black arrows indicate the hypoglossal nerve within the hypoglossal canal; open thick white arrow, supCNX; dotted white arrow, the dural septum between the petrosal and jugular part of the JF; 2, vertebral arteries. Note that a brain stem arteriovenous malformation is also present as an incidental finding in this patient (marked as 3). *B*, FIESTA images reconstructed in a considerably oblique plane aligned precisely along the anatomic course of the cisternal segment of the glossopharyngeal nerve root bundle (*dotted white arrows*) and the vagal nerve root bundle (*thin white arrows*). The crossed arrows mark supCNIX, whereas the thick open arrows delineate the supCNX. 1 indicates a meningeoma; 2, the vertebral artery.

appears to be weaker than the contrast provided by contrast-enhanced T1-weighted sequences such as 3D magnetization-prepared rapid acquisition of gradient echo and MRA.[8,15] For example, it has been shown that contrast-enhanced time-of-flight (TOF) MRA is a useful tool to image the trigeminal ganglion due to its strong venous enhancement.[15] Compared with TOF-MRA, CE-MRA is less prone to flow-related signal-intensity loss,[21] while also providing excellent arterial and venous contrast.[22] Here for the first time, we made use of high-resolution CE-MRA to image the cranial nerves and to compare it to CE-FIESTA for the depiction of the JF and its content.

Identification of CNIX, CNX, and CNXI within the JF

CNIX enters the JF through a dural channel called the glossopharyngeal meatus. Soon thereafter, CNIX abruptly turns forward and makes a 90° curve, the so-called genu of CNIX.[23] CNX and CNXI enter the JF together via the vagal meatus. This dural channel lies posterior to the glossopharyngeal meatus. The vagal meatus is located inferior to the glossopharyngeal meatus on the medial wall of the JF and is separated from the glossopharyngeal meatus by a dural septum.[23] At the dural orifice of the JF, the nerve roots of CNX and crCNXI intermingle; the 2 roots become indistinguishable and cannot be separated from each other by microdissection.[2] Thus, CNX and crCNXI are referred to as the CNX/XI complex.

CE-FIESTA and CE-MRA both provided excellent contrast and resolution within the JF. Both sequences could be used to identify the nerves as nonenhancing linear structures coursing through the surrounding enhancing venous structures. Both sequences could be used to differentiate between CNIX and the CNX/XI complex within the foramen. However, CE-MRA proved to be superior to CE-FIESTA in this respect, due to the stronger and more homogeneous contrast of the surrounding venous plexus provided by CE-MRA.

On the other hand, the CE-FIESTA provided excellent depiction of the cisternal courses of the cranial nerves. On CE-FIESTA sequences, the cranial nerves can be followed from their exit at the brain stem through the cisterns into their respective meatuses and through the JF. Therefore, both cisternal and intraforaminal nerve segments can be imaged by use of a single sequence. Thus, the CE-FIESTA facilitated the differentiation of spCNXI from the CNX/XI complex, which was not possible with the use of CE-MRA.

Our results support recent anatomic studies that question the presence of an intracisternal or intraforaminal connection between the crCNXI nerve root bundles and spCNXI and demonstrate a tight connection between CNX and crCNXI within the JF.[4,24]

Compartments of the JF

According to Rhoton,[1] the JF may be subdivided into 3 compartments: 1 neural or intrajugular compartment (pars nervosa) and 2 venous compartments, which are partially separated by the intrajugular processes of the temporal and occipital bones and by dural septa. The venous compartments consist of the larger posterolateral sigmoid compartment, which receives the flow of the sigmoid sinus, and a smaller anteromedial petrosal compartment, which receives drainage from the inferior petrosal sinus. The pars nervosa, which contains CNIX–CNXI, is situated between the sigmoid and petrosal compartments.[1,2]

In accordance with these anatomic findings, we could depict the intrajugular processes and the dural septum separating the petrosal from the sigmoid compartments. We found that the cranial nerves aligned between the venous compartments along a trajectory from anterolateral (CNIX) to posteromedial direction (first, the CNX/XI complex and, second, the spCNXI).

Cochlear Aqueduct

The cochlear aqueduct houses the perilymphatic duct and a tubular prolongation of the dura mater that is filled with CSF. The external opening of the aqueduct is located medial to the jugular fossa and above the level of the petrosal fossula. Thus, it lies immediately adjacent to the entrance porus of CNIX and just cranial to the supCNIX.[23] The cochlear aqueduct is widest where it lies closest to CNIX and narrows toward the cochlea.[25,26] CE-FIESTA was superior to CE-MRA in depicting the aqueduct, most probably due to the high signal intensity of CSF on CE-FIESTA. Anatomic dissection studies showed that the cochlear aqueduct is not patent in most cases (60%–67%[25]). Not surprisingly, therefore, CE-FIESTA studies, in vivo, showed the full

length of the aqueduct in only 27%. This difference most likely is the result of the difficulty of MR imaging in displaying the very narrow (0.1-mm-diameter) portion of the aqueduct near the cochlea.[26]

Ganglia

To the best of our knowledge, this is the first in vivo imaging study that assesses the visualization of the ganglia of CNX and CNX in detail.

The supCNIX is located within a small dural pocket just at the point where CNIX pierces the dura of the glossopharyngeal meatus. It has a mean diameter of 1.5 mm and is macroscopically visible as a circumscribed thickening of the nerve in only one third of cases.[1] Using the external opening of the cochlear aqueduct and the genu of CNIX as landmarks,[1,23] we identified the supCNIX on CE-FIESTA and CE-MRA in 90% and 88% of sides, respectively.

The infCNIX can be detected approximately 3 mm inferior to the supCNIX[3] and is the origin of the tympanic nerve (Jacobson nerve). CE-MRA was superior to the CE-FIESTA in visualizing the infCNIX (100% versus 73%). This is explained by the more homogeneous venous contrast in CE-MRA.

The supCNX is seen as an expansion of CNX just distal to where its rootlets gather at the intracranial side of the foramen. It is about 2.5 mm in length and ends at the extracranial side of the foramen.[1,2] We could always identify the CNX/XI complex at the anatomic site of this ganglion (score of 1), whereas we never observed a clearly defined thickening of the nerve. This is in accordance with the fact that the supCNX is macroscopically visible as a circumscribed thickening of the nerve in only one sixth of cases.[1] Both CE-MR imaging sequences depicted the supCNX well.

The auricular branch of CNX (Arnold nerve) arises from CNX at the level of the supCNX. Although Jacobson and Arnold nerves were not directly assessed in this study, the infCNIX and the supCNX provide landmarks for localizing the site of their origin. Because Arnold and Jacobson nerves may be related to glomus tumors, depiction of the sites of origin of these nerves could have clinical significance.[1,27] The inferior ganglion of CNX was not analyzed in this study because it is not located within the JF, but more caudally along the course of CNX.

Jugular Bulb and Inferior Petrosal Sinus

The jugular bulb and the JF are usually larger on the right side, reflecting the larger diameter of the sigmoid sinus on the right.[6,28] Accordingly, we found a significantly larger jugular bulb on the right side in 60% of cases, whereas the inferior petrosal sinus showed no significant difference in size from the left to right sides.

The inferior petrosal sinus interconnects the cavernous sinus and the basilar venous plexus with the jugular bulb and courses on the intracranial surface of the petroclival fissure. After entering the petrosal portion of the JF, the inferior petrosal sinus forms a plexiform confluence with the venous plexus of the hypoglossal canal, the inferior petroclival vein, and tributaries from the vertebral venous plexus and the posterior condylar emissary vein. This confluence empties into the medial aspect of the jugular bulb through 1 or 2 openings most often between CNIX and CNX.[1] CE-MRA enabled us to visualize the variations of this drainage into the jugular bulb. The mean width of the distal inferior petrosal sinus was determined to be 3.5 mm in our study, which is in accord with anatomic dissection studies (2–4 mm[29]).

Relationship to Adjacent Cranial Nerves

Several important anatomic structures traverse the skull base in close vicinity to the JF. These are namely the internal carotid artery (ICA) anteriomedially, the CNVII laterally, and the CNXII inferolaterally. Detailed knowledge of these spatial relationships is essential in neurosurgical approaches to the JF.[1]

CNXII joins CNIX-XI when exiting the JF and courses adjacent to the vagus nerve. The extracranial opening of the hypoglossal canal is typically located medial to the pars nervosa of the JF,[1] which could always be detected with both sequences equally well. CE-FIESTA and CE-MRA allowed detailed evaluation of the relationship between the CNXII and the nerves of the JF. In accordance with anatomic dissection studies,[30] we observed a duplicated canal in 10% of sides, a finding that has not yet been described in MR imaging studies.

CNVII crosses the lateral surface of the styloid process adjacent to the JF. The close spatial relationship between CNVII and the JF is of particular importance in the postauricular transtemporal approach, the most commonly used surgical route for lesions extending through the JF.[1] CE-MRA and particularly the CE-FIESTA sequence enabled us to visualize the CNVII in its complete course through the temporal bone to the parotid gland and thus might facilitate presurgical planning of lateral approaches.[1,2]

Limitations of the Protocol

One limitation of our protocol might be the duration of approximately 15 minutes if both sequences are performed. In patients with reduced compliance, this will probably result in a reduced imaging quality. In such cases, we recommend choosing one of the sequences, depending on the pathologic condition that is suggested. If the JF itself is affected, CE-MRA should be performed as the first line; if the pathology predominately affects the cisternal part of the lower cranial nerves, the FIESTA sequence should be chosen.

Implications for Patient Care

A wide variety of pathologic processes affect the JF (eg, glomus jugulare tumors, neurinomas, and meningiomas).[3,31] Furthermore, the nerves can be compromised iatrogenically during surgical treatment of such lesions.[23,32] Thus, detailed knowledge of the JF, its contents, and adjacent cranial nerves is important for both radiologists and neurosurgeons. On the basis of our findings, we propose the combined use of CE-FIESTA and CE-MRA as the ideal imaging protocol to depict the detailed in vivo anatomy of the JF, its content, and adjacent structures that might facilitate the planning of surgical approaches to that region. We included an illustrative case to provide evidence for the potential of these sequences (Fig 8). Further studies on patients with pathologies affecting the JF are necessary to prove the advantages of this protocol in clinical settings.

Conclusions

On the basis of our results, we propose the combined use of CE-FIESTA and CE-MRA sequences as optimal imaging protocol for the analysis of the JF and its contents at 3T. This protocol is expected to aid in detecting and characterizing pathologic conditions of the JF and in planning the best safe surgical approach to lesions in the JF region. Further studies on larger case series should be performed to confirm its value in pathologic conditions of the JF.

References

1. Rhoton AL. **Jugular foramen.** *Neurosurgery* 2000;47(suppl 3):267–85
2. Tekdemir I, Tuccar E, Aslan A, et al. **Comprehensive microsurgical anatomy of the jugular foramen and review of terminology.** *J Clin Neurosci* 2001;8:351–56
3. Song MH, Lee HY, Jeon JS, et al. **Jugular foramen schwannoma: analysis on its origin and location.** *Otol Neurotol* 2008;29:387–91
4. Lachman N, Acland RD, Rosse C. **Anatomical evidence for the absence of a morphologically distinct cranial root of the accessory nerve in man.** *Clin Anat* 2002;15:4–10
5. Rubinstein D, Burton BS, Walker AL. **The anatomy of the inferior petrosal sinus, glossopharyngeal nerve, vagus nerve, and accessory nerve in the jugular foramen.** *AJNR Am J Neuroradiol* 1995;16:185–94
6. Hatiboglu M, Anil A. **Structural variations in the jugular foramen of the human skull.** *J Anat* 1992;180:191–96
7. Lang J. **Jugular foramen**. In: Lang J, ed. *Clinical Anatomy of the Posterior Cranial Fossa and Its Foramina.* New York: Thieme Medical Publishers; 1991:92–96
8. Yousry I, Moriggl B, Schmid UD, et al. **Detailed anatomy of the intracranial segment of the hypoglossal nerve: neurovascular relationships and landmarks on magnetic resonance imaging sequences.** *J Neurosurg* 2002;96:1113–22
9. Davagnanam I, Chavda SV. **Identification of the normal jugular foramen and lower cranial nerve anatomy: contrast-enhanced 3D fast imaging employing steady-state acquisition MR imaging.** *AJNR Am J Neuroradiol* 2008;29:574–76. Epub 2007 Dec 7
10. Daniels DL, Williams AL, Haughton VM. **Jugular foramen: anatomic and computed tomographic study.** *AJR Am J Roentgenol* 1984;142:153–58
11. Lo WW, Solti-Bohman LG. **High-resolution CT of the jugular foramen: anatomy and vascular variants and anomalies.** *Radiology* 1984;150:743–47
12. Chong VF, Fan YF. **Radiology of the jugular foramen.** *Clin Radiol* 1998;53:405–16
13. Daniels DL, Schenck JF, Foster T, et al. **Magnetic resonance imaging of the jugular foramen.** *AJNR Am J Neuroradiol* 1985;6:699–703
14. Daniels DL, Czervianke LF, Pech P. **Gradient recalled echo MR imaging of the jugular foramen.** *AJNR Am J Neuroradiol* 1988;9:675–78
15. Yousry I, Moriggl B, Schmid UD, et al. **Trigeminal ganglion and its divisions: detailed anatomic MR imaging with contrast-enhanced 3D constructive interference in the steady state sequences.** *AJNR Am J Neuroradiol* 2005;26:1128–35
16. Yagi A, Sato N, Taketomi A, et al. **Normal cranial nerves in the cavernous sinuses: contrast-enhanced three-dimensional constructive interference in the steady state MR imaging.** *AJNR Am J Neuroradiol* 2005;26:946–50
17. Yousry I, Camelio S, Wiesmann M, et al. **Detailed magnetic resonance imaging anatomy of the cisternal segment of the abducent nerve: Dorello's canal and neurovascular relationships and landmarks.** *J Neurosurg* 1999;91:276–83
18. Casselman JW, Kuhweide R, Deimling M, et al. **Constructive interference in steady state-3DFT MR imaging of the inner ear and cerebellopontine angle.** *AJNR Am J Neuroradiol* 1993;14:47–57
19. Yousry I, Camelio S, Schmid UD, et al. **Visualization of cranial nerves I-XII: value of 3D CISS and T2-weighted FSE sequences.** *Eur Radiol* 2000;10:1061–67
20. Seitz J, Held P, Fründ R, et al. **Visualization of the IXth to XIIth cranial nerves using 3-dimensional constructive interference in steady state, 3-dimensional magnetization-prepared rapid gradient echo and T2-weighted 2-dimensional turbo spin echo magnetic resonance imaging sequences.** *J Neuroimaging* 2001;11:160–64
21. Wikström J, Ronne-Engström E, Gal G, et al. **Three-dimensional time-of-flight (3D TOF) magnetic resonance angiography (MRA) and contrast-enhanced MRA of intracranial aneurysms treated with platinum coils.** *Acta Radiol* 2008;49:190–96
22. Nael K, Fenchel M, Salamon N, et al. **Three-dimensional cerebral contrast-enhanced magnetic resonance venography at 3.0 Tesla: initial results using highly accelerated parallel acquisition.** *Invest Radiol* 2006;41:763–68
23. Ozveren MF, Türe U, Ozek MM, et al. **Anatomic landmarks of the glossopharyngeal nerve: a microsurgical anatomic study.** *Neurosurgery* 2003;52:1400–10
24. Ryan S, Blyth P, Duggan N, et al. **Is the cranial accessory nerve really a portion of the accessory nerve? Anatomy of the cranial nerves in the jugular foramen.** *Anat Sci Int* 2007;82:1–7
25. Gopen Q, Rosowski JJ, Merchant SN. **Anatomy of the normal human cochlear aqueduct with functional implications.** *Hear Res* 1997;107:9–22
26. Rask-Andersen H, Stahle J, Wilbrand H. **Human cochlear aqueduct and its accessory canals.** *Ann Otol Rhinol Laryngol Suppl* 1977;86:1–16
27. Guild SR. **Glomus jugulare, a nonchromaffin paraganglion in man.** *Ann Otol Rhinol Laryngol* 1953;62:1045–71
28. Dichiro G, Fisher RL, Nelson KB. **The jugular foramen.** *J Neurosurg* 1964;21:447–60
29. Lang J. **Veins and dural sinuses**. In: Von Lanz T, Wachsmuth W, eds. *Practical Anatomy: Part I—Head.* Berlin, Germany: Springer-Verlag; 2004:578–633
30. Bhuller A, Sanudo JR, Choi D, et al. **Intracranial course and relations of the hypoglossal nerve: an anatomic study.** *Surg Radiol Anat* 1998;20:109–12
31. Ramina R, Maniglia JJ, Fernandes YB, et al. **Tumors of the jugular foramen: diagnosis and management.** *Neurosurgery* 2005;57(suppl 1):59–68
32. Roche PH. Mercier P, Sameshima T, et al. **Surgical anatomy of the jugular foramen.** *Adv Tech Stand Neurosurg* 2008;33:233–63